metals

MDPI

Article

RBF-Neural Network Applied to the Quality Classification of Tempered 100Cr6 Steel Cams by the Multi-Frequency Nondestructive Eddy Current Testing

Víctor Martínez-Martínez [1,*], Javier Garcia-Martin [1,2] and Jaime Gomez-Gil [1]

1 Department of Signal Theory, Communications and Telematics Engineering, University of Valladolid, 47011 Valladolid, Spain; jgarmar@ribera.tel.uva.es or sensors.simulation@ isend.es (J.G.-M.); jgomez@tel.uva.es (J.G.-G.)

2 Ingeniería y Sistemas de Ensayos no Destructivos (ISEND), Boecillo Technological Park, Luis Proust 10, 47151 Valladolid, Spain

* Correspondence: vmarmar@ribera.tel.uva.es; Tel.: +34-636-797-528

Received: 18 August 2017; Accepted: 15 September 2017; Published: 21 September 2017

Abstract: This article proposes a Radial Basis Function Artificial Neural Network (RBF-ANN) to classify tempered steel cams as correctly or incorrectly treated pieces by using multi-frequency nondestructive eddy current testing. Impedances at five frequencies between 10 kHz and 300 kHz were employed to perform the binary sorting. The ANalysis Of VAriance (ANOVA) test was employed to check the significance of the differences between the impedance samples for the two classification groups. Afterwards, eleven classifiers were implemented and compared with one RBF-ANN classifier: ten linear discriminant analysis classifiers and one Euclidean distance classifier. When employing the proposed RBF-ANN, the best performance was achieved with a precision of 95% and an area under the Receiver Operating Characteristic (ROC) curve of 0.98. The obtained results suggest RBF-ANN classifiers processing multi-frequency impedance data could be employed to classify tempered steel DIN 100Cr6 cams with a better performance than other classical classifiers.

Keywords: nondestructive testing; eddy current; tempering process; radial basis function neural network; multi-frequency; analysis of variance

1. Introduction

Nondestructive testing (NDT) techniques are analysis methods employed to inspect samples without causing permanent damage or modifications to them. Eddy current testing has been one of the most popular NDT techniques, and has been widely implemented as an alternative to metallography [1] and indentation hardness tests [2]. Eddy current testing is based on Faraday's electromagnetic induction law, which was proposed in 1831, and on Hughes' experiments, which were performed in 1879. Hughes found changes in the properties of a coil when it approached metals with different electric conductivities and magnetic permeabilities. The usage of eddy current testing techniques has significantly increased since the 1950s in the aeronautical [3,4] and nuclear [5,6] industries, among others. In recent years, state-of-the-art electronic components and processors have been applied to build eddy current instrumentation [7–9]. Moreover, eddy current testing techniques have been employed to analyze materials: Konoplyuk predicted the matrix microstructure in ductile cast irons [10], Mercier et al. classified steel decarburizing samples [11], and Wrzuszczak et al. detected defects on conducting materials [12].

NDT techniques provide data that can be employed to decide, for example, if the predominant microstructure of an analyzed steel sample is martensite, that provide enough hardness to machinery

parts. This decision can be made either by a trained and experienced person or by an expert system. Artificial Neural Networks (ANNs) are processing tools inspired by the human nervous system, which can implement expert systems using their input-output mapping capability [13]. Various authors have combined ANNs and NDT techniques in the literature: Wang et al. employed a back propagation ANN to monitor the stress and the temperature of steel using the Barkhausen noise theory [14]; Sathiyasekar et al. proposed a system based on an ANN and fuzzy logic to predict the quality of the insulation system of rotating machines [15]; Silva et al. designed methods based on Multi-Layer Perceptron ANNs (MLP-ANNs) and Support Vector Machines to detect the sigma phase in duplex stainless steels analyzing induced magnetic field signals [16]; Lee et al. employed a backpropagation ANN to evaluate the quality of resistance spot welding using scanning acoustic microscopy [17]; Junyan et al. designed a MLP-ANN to detect subsurface defects in different materials using thermography [18]; Pérez-Benítez et al. proposed a feature selection algorithm to optimize a probabilistic ANN that classifies magnetic material samples using magnetic Barkhausen noise information [19]; Cao et al. employed a Radial Basis Function ANN (RBF-ANN) to evaluate wire ropes with eddy current inspection [20]; Xu et al. proposed a Kohonen ANN to predict the coating failure process cycles on steel plates using electrochemical impedance spectroscopy data [21]; Nunes et al. employed ultrasound signals to classify Ni-based alloy samples with a MLP-ANN [22]; and Wrzuszczak et al. combined the eddy current information with ANNs to detect cracks on conducting layers and on ferrous tubes [12].

The main objective of this article is to analyze the suitability of RBF-ANNs to classify tempered steel cams using multi-frequency impedance data acquired from eddy current NDT. To this end, the performance of the proposed RBF-ANN is compared with other classical classifiers. To reach the proposed objective, the following tasks were performed: (i) acquisition of multi-frequency eddy current impedances from two DIN 100Cr6 steel cam sets with different cooling processes; (ii) application of the ANalysis Of VAriance (ANOVA) test to analyze the suitability of the acquired impedances to classify the steel cams; (iii) classification with RBF-ANN, Linear Discriminant Analysis (LDA), and Euclidean distance classifiers (EDC); and (iv) comparison of the aforementioned classifiers considering the precision and the area under the Receiver Operating Characteristic (ROC) curve.

2. Theoretical Background

Eddy currents, which are also called Foucault currents, are electric currents induced by a variable magnetic field in a conductor. According to Faraday's law, an eddy current flow is generated in a piece of steel when a coil fed with AC current is approached, as Figure 1 shows [23–25].

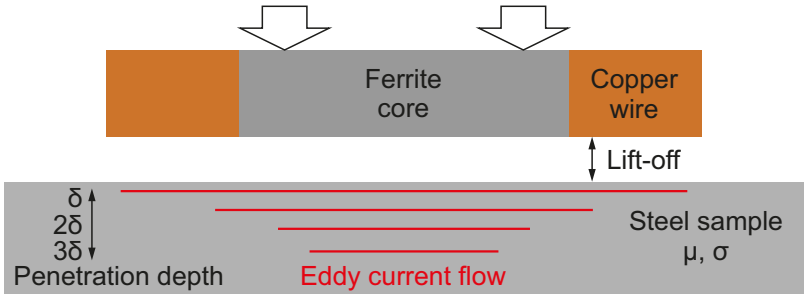

Figure 1. Eddy current flow generation approaching a ferrite-inductive coil probe to a steel sample. The main parameters involved are the lift-off, the penetration depth (δ), the magnetic permeability (μ), and the electrical conductivity (σ).

The magnitude and the phase of the induced eddy currents affect the loading of the coil and, thus, its global impedance Z_{coil}. The impedance of the coil is also affected by the lift-off, which is the separation between the coil and the steel sample. This impedance can be measured using an eddy current instrumentation device [25,26]. The coil excitation frequency f permits the adjustment of the

penetration depth δ, which is proportional to $f^{-0.5}$, according to the skin effect [27,28]. The acquired impedance of the coil Z_{coil} (x, σ, μ, f) is mainly related to the electrical conductivity σ, to the magnetic permeability μ, to the lift-off x, and to the applied and the residual stresses of the steel sample that slightly influence on σ and μ (Figure 2) [2,28].

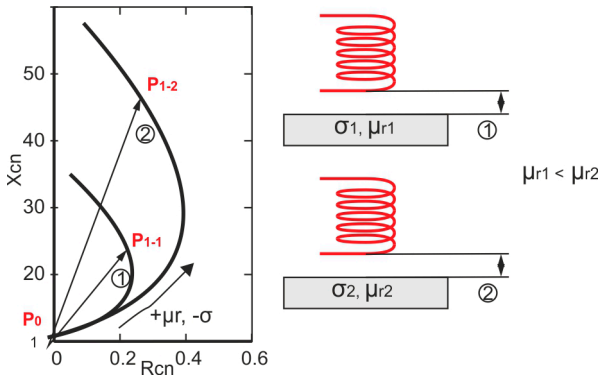

Figure 2. Normalized impedance plane to implement ferromagnetic samples sorting systems based on electrical conductivity σ_2–σ_1 and magnetic permeability μ_2–μ_1 variations.

3. Materials

The kit of eight DIN 100Cr6 steel cams for automobile engines shown in Figure 3 was employed to perform the NDT analysis presented in this article. These cams were heated up to 840–860 °C with an inductive method and cooled under different conditions, and then they were divided into two groups, Group 1 and Group 2. The cams belonging to Group 1 presented a hardness greater than 55 Hardness Rockwell-C (HRC) because they had been subjected to a rapid oil cooling in their manufacturing process (30–40 °C/s). The predominant metallurgical structure of the cams belonging to Group 1 was the desired martensite and some bainite. The cams belonging to Group 2 presented a hardness lower than 45 HRC because they had been subjected to a cooling process (20–30 °C/s) slower than the process of Group 1. The predominant metallurgical structure of the cams belonging to Group 2 was perlite and some bainite.

Figure 3. Image of the steel cams employed in the experiments: the four cams of the lower row (Group 1) had a predominant microstructure of martensite and a hardness greater than 55 HRC, while the four cams of the upper row (Group 2) had a predominant microstructure of perlite and a hardness lower than 45 HRC.

4. Methods

The methodology comprised five stages: impedance acquisition, data preprocessing, statistical analysis, classification, and ROC analysis, as Figure 4 shows.

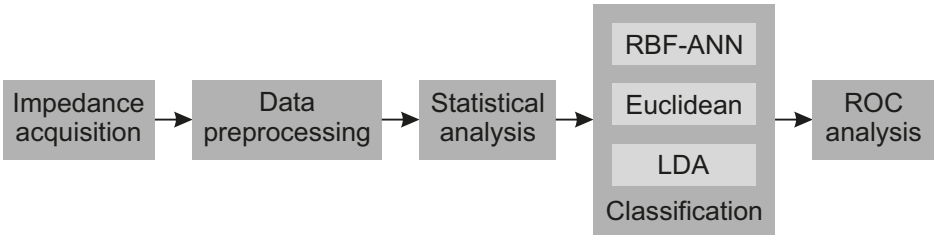

Figure 4. Block diagram of the methodology employed in this article.

The impedance acquisition stage was performed in lab conditions for its subsequent analysis. The acquired data were preprocessed in order to adapt them to the classifiers input requirements. These preprocessed data were analyzed with the ANOVA statistical test to evaluate if there were statically significant differences on the analyzed variables depending on the cooling conditions. After that, each analyzed cam was classified considering different classifiers, evaluating the performance of each classifier and performing a ROC analysis. A general purpose laptop (ASUSTeK Computer Inc., Taipei, Taiwan) with an Intel Core i3 M350 @ 2.27 GHz processor and 4 GB RAM was employed to perform the processing tasks of all the stages of the methodology.

4.1. Impedance Acquisition Stage

The impedance acquisition stage was performed using one coil probe, one ISEND CompAnalyzer device, and the abovementioned computer. The elements employed in the impedance acquisition stage are shown in Figure 5.

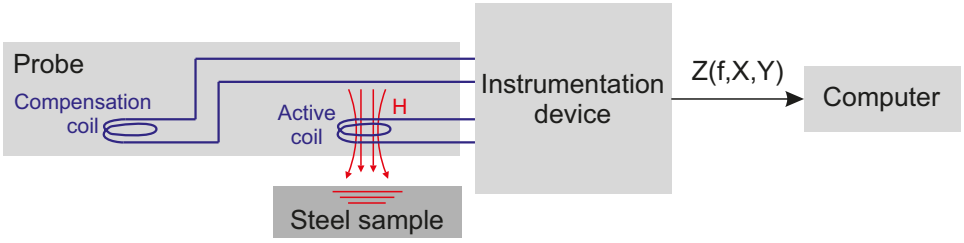

Figure 5. Layout of the elements employed in the impedance acquisition stage: the probe with an active and compensation coil, which generates an eddy current flow in a steel sample; the ISEND instrumentation device feed that measures the impedance $Z(f,X,Y)$; and the computer stores and processes the impedance values.

The probe was composed of one active-coil (a-c) with impedance $Z_{a\text{-}c}$ and one compensation coil (c-c) with impedance $Z_{c\text{-}c}$. The absolute with compensation operation mode was chosen for the probe in order to increase its dynamic range. The Wheatstone bridge represented in Figure 6 was employed to interconnect the probe with the instrumentation device.

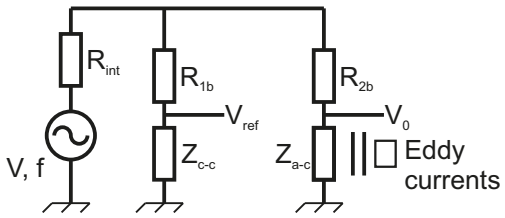

Figure 6. Wheatstone bridge interconnection of the absolute with a compensation coil probe, with impedances $Z_{a\text{-}c}$ and $Z_{c\text{-}c}$, to the instrumentation device.

The coils resistance (R) and inductance (L) values, and the resistance and inductance relative variations between active and compensating coils due to the manufacturing process are presented in Table 1. A reactance (XL) to resistance ratio greater than 1 warrantied operation in the 1–300 kHz frequency band, and resistance and inductance variations lower than 5% due to the manufacturing process, were considered acceptable.

Table 1. Resistance (R), inductance (L), reactance (XL), and impedance (Z) of active and compensating coils, and R and L relative variations between active and compensating coils at frequencies (f) 0.1 kHz, 0.12 kHz, 1 kHz, 10 kHz, and 100 kHz.

Active Coil					
f (kHz)	0.1	0.12	1	10	100
L (mH)	2.1415	2.1415	2.1308	2.1311	2.5888
XL (Ω)	1.3455	1.6147	13.3882	133.9010	1626.5910
R (Ω)	12.9030	12.9020	12.9000	12.8980	12.8930
Z (Ω)	12.9730	13.0026	18.5918	134.5207	1626.6421
Compensating Coil					
f (kHz)	0.1	0.12	1	10	100
L (mH)	2.1216	2.1187	2.1095	2.1071	2.5317
XL (Ω)	1.3330	1.5975	13.2544	132.3930	1590.7140
R (Ω)	12.4950	12.4980	12.5000	12.5010	12.5020
Z (Ω)	12.5659	12.5997	18.2189	132.9819	1590.7632
Active/Compensating *R*, *L* Coil Variation					
R variation	−3.1621%	−3.1313%	−3.1008%	−3.0780%	−3.0327%
L variation	−0.9293%	−1.0647%	−0.9996%	−1.1262%	−2.2057%

The ISEND CompAnalyzer device was employed to feed the probe at the desired frequency f and amplitude V, and to acquire the real and imaginary parts of the impedance ($\mathrm{Re}\{Z_{a\text{-}c}\}$ and $\mathrm{Im}\{Z_{a\text{-}c}\}$ respectively) from the acquired signal V_0–V_{ref} (Figure 6).

Impedance data were acquired at room temperature (23 °C) by approaching the steel cams to the coil probe (Figure 7), which was powered at one of the five different operating frequencies considered: 300 kHz, 100 kHz, 50 kHz, 20 kHz, and 10 kHz. The impedance was acquired with a lift-off lower than 0.2 mm, acquiring five measurements for each steel cam. These data were divided into two datasets: a training dataset, which contained the data of 50% of the cams, and the testing dataset, which contained the data of the remaining 50% of the cams. From this point forward, we will refer to these impedance components as 300R, 300X, 100R, 100X, 050R, 050X, 020R, 020X, 010R, and 010X, where the number refers to the acquisition frequency in kHz and the letter indicates if it refers to the resistance (R) or the reactance (X) of the impedance.

Figure 7. Image of the impedance acquisition procedure during the eddy current nondestructive tests.

4.2. Data Preprocessing Stage

Acquired impedance components were normalized to adapt them to the input required by the implemented classifiers [29]. The normalization procedure adjusted the mean value and the standard deviation of the data to zero and one, respectively, using the equation presented in (1):

$$Z'_i = R'_i + j \cdot X'_i \text{ where} \begin{cases} R'_i = \frac{R_i - \mu_R}{\sigma_R} \\ X'_i = \frac{X_i - \mu_X}{\sigma_X} \end{cases} \quad (1)$$

where μ_R and σ_R are, respectively, the mean and the standard deviation of the real part of the impedance values of the training dataset, and μ_X and σ_X are, respectively, the mean and the standard deviation of the imaginary part of the impedance values of the training dataset.

4.3. Statistical Analysis Stage

The one-way ANOVA test is a statistical procedure to analyze two or more groups of data. It performs statistical hypothesis testing considering that the means of the analyzed groups are the same as the null hypothesis. As a result, the ANOVA test gives a *p*-value, which is the probability that the analyzed data are drawn from populations with the same mean. In our work, a one-way ANOVA test was performed to analyze the statistical significance of the differences between the preprocessed impedance samples of the two classification groups considered. The *p*-value of each variable was obtained and compared with a significance level of $\alpha = 0.01$. According to the ANOVA test theory, *p*-values lower than α denote significant differences between the analyzed groups, while *p*-values greater than α denote non-significant differences [30].

4.4. Classification Stage

Twelve classifiers were implemented: one RBF-ANN, 10 LDA classifiers, and one EDC. The RBF-ANN classifier proposed in this article was compared with the 10 LDA classifiers, and with the EDC. LDA and EDC were chosen because they are, respectively, one-dimensional and multidimensional classifiers typically employed in the literature [31–33]. As LDA are one-dimensional classifiers, 10 LDA classifiers were considered to analyze the 10 variables considered by the RBF-ANN and the EDC. All the implemented classifiers employed impedance data as inputs, so none of them implemented a feature extraction stage before the classification stage.

4.4.1. RBF-ANN Classifier

An RBF-ANN with a single hidden layer was proposed to classify the steel cams. The input layer was composed of 10 neurons, which got the real and imaginary values of the impedances acquired at the five different frequencies under consideration. The number of hidden neurons was set to the number of training samples, which was 20, and the number of output neurons was set to 1. Each input sample was assigned to Group 1 or to Group 2 when the output was greater or lower than a threshold value respectively. Figure 8 shows a schematic of the proposed RBF-ANN.

The training method of the RBF-ANN consisted of two steps: (1) setting the weights of the hidden layer as the values of the training samples; and (2) adjusting the output layer weights and biases by means of solving the linear expression that relates the output of the hidden layer and the target values of the training samples [34–36].

4.4.2. LDA Classifiers

Ten LDA classifiers were proposed to classify the steel samples using independently each one of the ten acquired and preprocessed impedance components. The training method of the LDA classifiers consisted of the adjustment of the threshold, selecting the one that obtained the best classification rate with the training samples [37]. Each classifier was named LDA-FFFC, where FFFC referred to

the impedance component associated with the LDA classifier, using the nomenclature defined in Section 4.1.

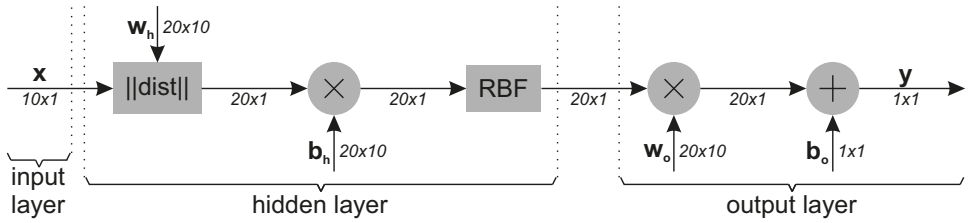

Figure 8. Schematic of the Radial Basis Function Artificial Neural Network (RBF-ANN) classifier proposed with 10 inputs, one hidden layer with 20 neurons, and one output. In this representation, x represents the input vector, y the output vector, w the weights vector, and b the biases vector. The h and o sub-indexes were used to refer to the hidden layer and the output layer respectively. The number beside each arrow indicates the size of the matrix data on this point of the ANN.

4.4.3. Euclidean Distance Classifier

EDC is a multidimensional classifier that assigns a sample to the group whose multi-frequency descriptive point, which is called centroid, is closer. The training method of the EDC consisted of calculating the centroids of the two groups of samples, called $\overline{c^{\mathrm{I}}}$ and $\overline{c^{\mathrm{II}}}$, as the average of the training samples of each group.

The trained EDC computed the Euclidean distance from the sample point to each centroid, evaluated the difference between the distances from the point to the two centroids $||\overline{x} - \overline{c^{\mathrm{I}}}|| - ||\overline{x} - \overline{c^{\mathrm{II}}}||$, and assigned the sample to Group 1 or to Group 2 when the difference was lower or higher than the threshold value respectively.

4.5. ROC Analysis Stage

The ROC analysis consisted in analyzing the performance of the classifiers described in the previous subsection as a function of their thresholds [13,38]. Three performance parameters were calculated in the ROC analysis: sensitivity, specificity, and precision. Sensitivity is the success rate considering only samples of Group 2, which is known as true positive rate. Specificity is the success rate considering only samples of Group 1, which is known as false positive rate. Precision is the success rate considering samples of both groups. The main graphical result of the ROC analysis is the ROC curve, which is a function that represents the sensitivity versus the specificity of the analyzed classifier for different values of the threshold. The main numerical result of the ROC analysis is the Area under the ROC curve (A_{ROC}). The optimum precision, which is the maximum precision that can be obtained with the analyzed classifier, is another numerical result commonly employed to describe the classifier.

5. Results

The results of the ANOVA test and the performance comparison of the implemented classifiers are presented in the next two subsections.

5.1. ANOVA Test Results

The ANOVA test was applied separately to each one of the 10 impedance components considered in order to evaluate the capability of these 10 variables to distinguish the two groups of samples with different heat treatment. The results obtained after applying the ANOVA test are shown in Table 2, presenting the p-value for each impedance component.

Considering a significance level of $\alpha = 0.01$, Table 2 shows that only impedance components $100R$, $020X$, and $010X$ had a p-value greater than α, while the other seven components had a p-value lower than α. According to the ANOVA test theory, the aforementioned three impedance components did

not have significant differences between the samples belonging to Groups 1 and 2, while the other seven impedance components had significant differences.

Table 2. ANOVA *p*-value of each impedance component.

Impedance Component	*p*-Value
300*R*	3.177×10^{-9}
300*X*	1.645×10^{-7}
100*R*	4.087×10^{-1}
100*X*	1.095×10^{-8}
050*R*	2.030×10^{-5}
050*X*	3.427×10^{-5}
020*R*	1.399×10^{-8}
020*X*	5.064×10^{-2}
010*R*	3.699×10^{-3}
010*X*	9.146×10^{-1}

5.2. Classifiers Performance Results

The twelve classifiers abovementioned were implemented and their performance was compared considering the testing dataset. To this end, the optimum precision, the ROC, and the A_{ROC} of each classifier were calculated in order to perform the comparison. The obtained results are shown in Table 3 and Figure 9.

Table 3. Optimum precision and Area under the Receiver Operating Characteristic (A_{ROC}) curve obtained for the Linear Discriminant Analysis (LDA), Euclidean distance classifiers (EDC), and RBF-ANN classifiers obtained for the classification performed with the testing dataset.

Classifier	Optimum Precision	A_{ROC}
RBF-ANN	95%	0.98
LDA-300*R*	90%	0.93
LDA-300*X*	80%	0.86
LDA-100*R*	70%	0.64
LDA-100*X*	90%	0.93
LDA-050*R*	75%	0.82
LDA-050*X*	80%	0.79
LDA-020*R*	85%	0.91
LDA-020*X*	70%	0.67
LDA-010*R*	75%	0.74
LDA-010*X*	55%	0.49
EDC	90%	0.96

According to Table 3, the RBF-ANN proposed in this article showed the best classification performance, with an optimum precision of 95% and an A_{ROC} of 0.98. The second-best classification performance was achieved by the EDC, with an optimum precision of 90% and an A_{ROC} of 0.93.

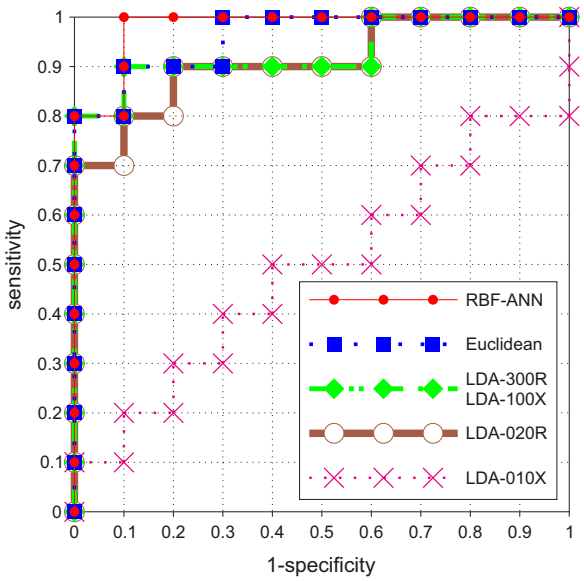

Figure 9. Schematic ROC curves for the LDA-300*R* (green), LDA-100*X* (green), LDA-020*R* (brown), LDA-010*X* (pink), EDC (blue), and RBF-ANN (red) classifiers obtained for the cams classification performed. The *X*-axis value (1-specificity) is the complementary of the specificity, and the *Y*-axis value is the sensitivity, both of them expressed as a real number between 0 and 1.

6. Discussion

The results presented in the previous section show two main findings. The first is that the proposed RBF-ANN can implement a method to classify tempered cams with high precision and high A_{ROC}. This finding is supported by the results presented in Table 3 for the RBF-ANN classifier, which show a precision of 95% in the steel samples classification. The second finding is that the RBF-ANN had a better performance than the other classifiers implemented in this article. This is supported by the results presented in Table 3, which show that the RBF-ANN obtained a precision and an A_{ROC} 5% and 2% higher than the best precision and A_{ROC} obtained by the LDA classifiers and the EDC.

The frequency range of the impedances employed as input values for the classifiers was between 10 kHz and 300 kHz, which are the frequencies associated to a penetration depth range between 20 µm and 102 µm according to the skin effect [27]. This penetration depth range inspects only the treated layer, which is greater than 500 µm, and provides enough impedance variation to classify the samples. The five considered frequencies, which where 10 kHz, 20 kHz, 50 kHz, 100 kHz, and 300 kHz, were chosen to sample as uniformly as possible both the frequency range and the penetration depth range in order to minimize common features of bainite between cams of Group 1 and Group 2 and remark the different features of martensite or perlite. Authors consider that the chosen frequencies were suitable for two reasons. On the one hand, the ANOVA test performed on the data used in this article showed 70% of components had significant differences between the two groups considered. This result suggests that the chosen frequency range is suitable to differentiate groups of samples with different cooling ramps. Pulsed eddy current testing could also be tested instead of the presented stationary testing [39], but the required transient response or magnitude spectrum analysis would have increased the RBF-ANN complexity. On the other hand, the frequency ranges employed in this article are in line with the work of other authors who chose similar frequency ranges in their research works. For example, Konoplyuk [10] employed impedances at several kHz to estimate the perlite composition in ductile cast irons, and Mercier et al. [11] and Habiby et al. [40] evaluated steel properties employing data in the range of a few kHz.

There are three noteworthy observations when analyzing the performance of the classifiers. The first observation is that the best classifiers considering the precision, are also the best classifiers

considering the A_{ROC}. It indicates that the classification ranking considering the precision is going to be the same ranking when considering the A_{ROC}. The second observation is the performance improvement of the RBF-ANN and the EDC compared to the LDA classifiers. This improvement could appear because the information necessary to perform the classification was not contained in a singular impedance component. Using multiple variables to improve the performance of univariate classifiers is common for both NDT field classifications [13], and general classification problems [35,36]. This is one of the possible reasons why classifiers with multiple inputs are mostly employed in the literature [31]. The third observation is the relation between the *p*-values of the ANOVA test and the classification results obtained by the LDA classifiers; the LDA classifier implemented for the impedance components with the highest *p*-values obtained the worst classification results and vice versa.

ROC analysis shows the performance of the proposed classifiers when having the best precision is not the main requirement to design the classifier. For example, some quality control applications require an optimum sensitivity in order to not classify one bad sample as a good one. When analyzing Figure 9, the specificity and precision of the classifiers with 100% sensitivity is, respectively, 90% and 95% for the RBF-ANN classifier, 40% and 80% for the best LDA classifier, and 70% and 85% for the EDC. The higher specificity and precision of the proposed RBF-ANN classifier compared to the EDC and LDA classifiers show the strength of the proposed classifier when different design conditions are considered.

One limitation of the presented work is related to the conditions in which the experiments have been performed. Data acquisition was done in an experimental laboratory with a controlled ambient temperature and away from noise sources, while industrial data acquisition is usually performed with variable ambient temperature and external noise sources. Nevertheless, the external noise influences could be minimized with a filtering stage, and the temperature changes influence in the measurements is expected to be reduced because of the self-compensating coil. Another limitation is that the proposed method has been validated only for the analyzed steel cams considering only two different cooling conditions. However, the theoretical basis of the proposed classification method suggests that a similar method could be applied when other steel pieces or other cooling conditions are considered. Moreover, using RBF-ANNs will facilitate solving the problems derived from these two limitations thanks to its adaptivity capability, which eases its retraining process when minor changes in the conditions are considered [35]. The third limitation of the presented work is that the implemented classifiers have not yet been implemented in a quality control line to test its performance in real conditions. Nevertheless Garcia-Martin et al. [41] found that a MLP-ANN without a feature extraction stage can classify steel cams with an execution time small enough to not consider the processing time as a limiting factor. This finding suggests that the processing time is not an important issue in the classification system proposed in this article.

The results obtained in this work suggest some research lines that could be conducted in the future. On the one hand, the proposed classification method could be improved considering more realistic industrial conditions, such as variable air temperature, the presence of conducted or radiated electric noise, or high speed classification requirements. On the other hand, the proposed methodology could be applied considering other factors, such as other tempering cycles, other types of steel, or fusing the considered eddy current data with pulsed eddy current testing [42] or another NDT techniques data to improve the classification performance.

7. Conclusions

This study suggests two conclusions about employing an RBF-ANN to classify tempered DIN 100Cr6 cams using multi-frequency NDT eddy current impedance data. The first is that a classifier based on an RBF-ANN can perform the classification with good precision and A_{ROC}, 95% and 0.98 respectively in our test. The second is that RBF-ANN-based classifiers achieve higher performance than other classifiers, such as LDA and EDC, with at least a precision of 5% higher and an A_{ROC} of 2% higher in our test. Obtained results show that eddy current impedance data acquired at different

frequencies can be used to distinguish between the two analyzed tempering conditions with good precision, with RBF-ANNs being a good classification method to process this multi-frequency data. Furthermore, the aforementioned conclusions suggest that the proposed method can be employed to classify DIN 100Cr6 cams in a quality point of the production line.

Acknowledgments: The authors thank the company Ingeniería y Sistemas de Ensayos no Destructivos ISEND (www.isend.es/en) for the valuable help in the experimental tests. The first author's work was also possible thanks to a "Formación de Personal Investigador" program grant. This program was financed by the "Universidad de Valladolid" (Spain) and co-financed by "Banco Santander". The authors would also like to thank the Writing Center of the University of Kentucky (USA) for their help reviewing this article.

Author Contributions: Víctor Martínez-Martínez, Javier Garcia-Martin and Jaime Gomez-Gil conceived and designed the experiments; Javier Garcia-Martin performed the data acquisition experiments; Víctor Martínez-Martínez processed and analyzed the data under the supervision of Javier Garcia-Martin and Jaime Gomez-Gil; Javier Garcia-Martin and Jaime Gomez-Gil wrote collaboratively the paper.

Conflicts of Interest: The authors declare no conflict of interest.

References

1. Khan, S.; Ali, F.; Khan, A.N.; Iqbal, M. Pearlite determination in plain carbon steel by eddy current method. *J. Mater. Process. Technol.* **2008**, *200*, 316–318. [CrossRef]
2. Zergoug, M.; Lebaili, S.; Boudjellal, H.; Benchaala, A. Relation between mechanical microhardness and impedance variations in eddy current testing. *NDT E Int.* **2004**, *37*, 65–72. [CrossRef]
3. Le Diraison, Y.; Joubert, P.-Y.; Placko, D. Characterization of subsurface defects in aeronautical riveted lap-joints using multi-frequency eddy current imaging. *NDT E Int.* **2009**, *42*, 133–140. [CrossRef]
4. He, Y.; Luo, F.; Pan, M.; Weng, F.; Hu, X.; Gao, J.; Liu, B. Pulsed eddy current technique for defect detection in aircraft riveted structures. *NDT E Int.* **2010**, *43*, 176–181. [CrossRef]
5. Yusa, N.; Janousek, L.; Rebican, M.; Chen, Z.; Miya, K.; Chigusa, N.; Ito, H. Detection of embedded fatigue cracks in Inconel weld overlay and the evaluation of the minimum thickness of the weld overlay using eddy current testing. *Nucl. Eng. Des.* **2006**, *236*, 1852–1859. [CrossRef]
6. Yusa, N.; Machida, E.; Janousek, L.; Rebican, M.; Chen, Z.; Miya, K. Application of eddy current inversion technique to the sizing of defects in Inconel welds with rough surfaces. *Nucl. Eng. Des.* **2005**, *235*, 1469–1480. [CrossRef]
7. Betta, G.; Ferrigno, L.; Laracca, M. GMR-based ECT instrument for detection and characterization of crack on a planar specimen: A hand-held solution. *IEEE Trans. Instrum. Meas.* **2012**, *61*, 505–512. [CrossRef]
8. Bernieri, A.; Ferrigno, L.; Laracca, M.; Molinara, M. Crack shape reconstruction in eddy current testing using machine learning systems for regression. *IEEE Trans. Instrum. Meas.* **2008**, *57*, 1958–1968. [CrossRef]
9. Simm, A.; Theodoulidis, T.; Poulakis, N.; Tian, G.Y. Investigation of the magnetic field response from eddy current inspection of defects. *Int. J. Adv. Manuf. Technol.* **2011**, *54*, 223–230. [CrossRef]
10. Konoplyuk, S. Estimation of pearlite fraction in ductile cast irons by eddy current method. *NDT E Int.* **2010**, *43*, 360–364. [CrossRef]
11. Mercier, D.; Lesage, J.; Decoopman, X.; Chicot, D. Eddy currents and hardness testing for evaluation of steel decarburizing. *NDT E Int.* **2006**, *39*, 652–660. [CrossRef]
12. Wrzuszczak, M.; Wrzuszczak, J. Eddy current flaw detection with neural network applications. *Measurement* **2005**, *38*, 132–136. [CrossRef]
13. Gros, X. *NDT Data Fusion*; Elsevier: Amsterdam, The Netherlands, 1996.
14. Wang, P.; Zhu, L.; Zhu, Q.; Ji, X.; Wang, H.; Tian, G.; Yao, E. An application of back propagation neural network for the steel stress detection based on Barkhausen noise theory. *NDT E Int.* **2013**, *55*, 9–14. [CrossRef]
15. Sathiyasekar, K.; Thyagarajah, K.; Krishnan, A. Neuro fuzzy based predict the insulation quality of high voltage rotating machine. *Expert Syst. Appl.* **2011**, *38*, 1066–1072. [CrossRef]
16. Silva, E.; Marinho, L.; Filho, P.; Leite, J.; Leite, J.; Fialho, W.; de Albuquerque, V.; Tavares, J. Classification of induced magnetic field signals for the microstructural characterization of sigma phase in duplex stainless steels. *Metals* **2016**, *6*, 164. [CrossRef]

17. Lee, H.-T.; Wang, M.; Maev, R.; Maeva, E. A study on using scanning acoustic microscopy and neural network techniques to evaluate the quality of resistance spot welding. *Int. J. Adv. Manuf. Technol.* **2003**, *22*, 727–732. [CrossRef]
18. Junyan, L.; Qingju, T.; Xun, L.; Yang, W. Research on the quantitative analysis of subsurface defects for non-destructive testing by lock-in thermography. *NDT E Int.* **2012**, *45*, 104–110. [CrossRef]
19. Pérez-Benitez, J.A.; Padovese, L.R. Feature Selection and Neural Network for analysis of microstructural changes in magnetic materials. *Expert Syst. Appl.* **2011**, *38*, 10547–10553. [CrossRef]
20. Cao, Q.; Liu, D.; He, Y.; Zhou, J.; Codrington, J. Nondestructive and quantitative evaluation of wire rope based on radial basis function neural network using eddy current inspection. *NDT E Int.* **2012**, *46*, 7–13. [CrossRef]
21. Xu, Y.; Ran, J.; Chen, H. Kohonen Neural Network Classification for Failure Process of Metallic Organic Coating in Corrosion Environment. *Metals* **2017**, *7*, 147.
22. Nunes, T.M.; de Albuquerque, V.H.C.; Papa, J.P.; Silva, C.C.; Normando, P.G.; Moura, E.P.; Tavares, J.M.R.S. Automatic microstructural characterization and classification using artificial intelligence techniques on ultrasound signals. *Expert Syst. Appl.* **2013**, *40*, 3096–3105. [CrossRef]
23. Mix, P.E. *Introduction to Nondestructive Testing: A Training Guide*; John Wiley & Sons: Hoboken, NJ, USA, 2005.
24. Davis, J.R. *ASM Handbook: Nondestructive Evaluation and Quality Control*; ASM International: Novelty, OH, USA, 1989; Volume 17.
25. Qu, Z.; Zhao, Q.; Meng, Y. Improvement of sensitivity of eddy current sensors for nano-scale thickness measurement of Cu films. *NDT E Int.* **2014**, *61*, 53–57. [CrossRef]
26. Dodd, C.; Deeds, W. Analytical Solutions to Eddy-Current Probe-Coil Problems. *J. Appl. Phys.* **1968**, *39*, 2829–2838. [CrossRef]
27. Garcia-Martin, J.; Gomez-Gil, J.; Vazquez-Sanchez, E. Non-destructive techniques based on eddy current testing. *Sensors* **2011**, *11*, 2525–2565. [CrossRef] [PubMed]
28. Tian, G.; Zhao, Z.; Baines, R. The research of inhomogeneity in eddy current sensors. *Sens. Actuators A Phys.* **1998**, *69*, 148–151. [CrossRef]
29. Deza, M.M.; Deza, E. *Encyclopedia of Distances*; Springer: Berlin, Germany, 2009.
30. Scheffe, H. *The Analysis of Variance*; John Wiley & Sons: Hoboken, NJ, USA, 1999; Volume 72.
31. Duda, R.O.; Hart, P.E.; Stork, D.G. *Pattern Classification*; John Wiley & Sons: Hoboken, NJ, USA, 2012.
32. Marco, V.R.; Young, D.M.; Turner, D.W. The Euclidean distance classifier: An alternative to the linear discriminant function. *Commun. Stat. Simul. Comput.* **1987**, *16*, 485–505. [CrossRef]
33. Zhao, W.; Chellappa, R.; Nandhakumar, N. Empirical performance analysis of linear discriminant classifiers. In Proceedings of the 1998 IEEE Computer Society Conference on Computer Vision and Pattern Recognition, Santa Barbara, CA, USA, 23–25 June 1998; pp. 164–169.
34. Broomhead, D.S.; Lowe, D. *Radial Basis Functions, Multi-Variable Functional Interpolation and Adaptive Networks*; DTIC Document; Royal Signals and Radar Establishment Malvern (United Kingdom): London, UK, 1988.
35. Haykin, S. *Neural Networks: A Comprehensive Foundation*; Prentice Hall PTR: Upper Saddle River, NJ, USA, 1998; p. 842.
36. Bishop, C.M. *Neural Networks for Pattern Recognition*; Oxford University Press: Oxford, UK, 2007.
37. Webb, A.R. *Statistical Pattern Recognition*; John Wiley & Sons: Hoboken, NJ, USA, 2003.
38. Fawcett, T. An introduction to ROC analysis. *Pattern Recognit. Lett.* **2006**, *27*, 861–874. [CrossRef]
39. Adewale, I.D.; Tian, G.Y. Decoupling the influence of permeability and conductivity in pulsed eddy-current measurements. *IEEE Trans. Magn.* **2013**, *49*, 1119–1127. [CrossRef]
40. Habiby, F.; Siddiqui, T.; Khan, S.; Khan, A. Austenite determination by eddy current measurements in a maraging steel. *NDT E Int.* **1992**, *25*, 145–146. [CrossRef]
41. Garcia-Martin, J.; Martínez-Martínez, V.; Gomez-Gil, J. Heat-treatment classification of steels with nondestructive eddy current testing using neural networks. *Dyna* **2014**, *89*, 526–532.
42. Chen, X.; Lei, Y. Electrical conductivity measurement of ferromagnetic metallic materials using pulsed eddy current method. *NDT E Int.* **2015**, *75*, 33–38. [CrossRef]